Received 25 October 2020; revised 24 November 2020; accepted 24 November 2020. Date of publication 2 December 2020;
date of current version 15 January 2021.

Digital Object Identifier 10.1109/OJAP.2020.3041953

Review on Ray Tracing Channel Simulation Accuracy in Sub-6 GHz Outdoor Deployment Scenarios

ALLAN WAINAINA MBUGUA [1,2], YUN CHEN [1], LESZEK RASCHKOWSKI [3], LARS THIELE [3], STEPHAN JAECKEL [3] (Member, IEEE), AND WEI FAN [2] (Senior Member, IEEE)

[1]Huawei Technologies Duesseldorf GmbH, Munich Research Center, 80992 Munich, Germany

[2]Antennas, Propagation and Millimetre-Wave Systems Section, Aalborg University, 9220 Aalborg, Denmark

[3]Fraunhofer Institute for Telecommunications, Heinrich Hertz Institute, 10587 Berlin, Germany

CORRESPONDING AUTHOR: W. FAN (e-mail: wfa@es.aau.dk)

ABSTRACT In this article, a review of the achieved accuracy in the literature for ray tracing (RT) based channel modeling is presented with a focus on outdoor propagation scenarios in the sub-6 GHz frequency range. The achieved accuracy is analyzed from three perspectives: 1) The input parameters which include the environmental description in the form of digital maps and the corresponding constitutive material parameters; 2) from the interaction mechanisms perspective and 3) from the output perspective where the achieved accuracy of predicted path loss is reviewed. Uniform assignment of materials to the entire propagation scenario is observed in most of the works in the literature which is attributed to the composite nature of common building materials and the difficulty of characterizing all material properties especially for outdoor scenarios. The digital maps are shown to introduce a certain degree of uncertainty in the RT predictions as most common sources of the maps hardly publish the accuracy. Notwithstanding, the prediction of path loss in most RT tools is observed to be rather robust against the inaccuracies in the input parameters with most RT tools achieving a prediction accuracy with a mean error below 4 dB and a standard deviation (STD) below 8 dB.

INDEX TERMS Constitutive material parameters, digital maps, radio channel modeling, ray tracing, sub-6 GHz.

I. INTRODUCTION

ACCURATE channel models are critical for optimization of wireless communication systems. Deterministic channel models and in particular ray tracing (RT) have been employed for site-specific channel prediction from sub-6 GHz, millimeter-wave (mm-wave) and up to terahertz frequencies [1]–[4]. The attractiveness of the RT based approach is that it reduces the need for channel measurements which is often costly and time intensive [5]. This is in particular advantageous for network planning and coverage prediction purposes. The wide adoption of RT channel models in the past was mainly hindered by limited computational resources. The advancement of state-of-the-art computation techniques using graphical processing units has accelerated the use of RT channel models as simulations can be carried out within reasonable computational time [6]–[10]. RT channel models have indeed been recently used in novel applications such as virtual drive testing [11], [12], radio coverage simulation [5] and vehicular communications [13]–[16].

The generation of accurate site-specific channel models deterministically using RT is a non-trivial process. In most cases, all the information about a propagation scenario that affects the electromagnetic wave interaction with the environment is rarely available which requires some approximations to be carried out. Moreover, simplifications have also to be made to minimize the computational complexity. This could negatively impact the accuracy of the predicted channel hence validation of RT tools is fundamental to determine the fidelity of predicted channel parameters. In the literature, validation of RT channel models has mainly been performed via extensive channel sounding campaigns and then comparing the RT tools output parameters to the measured channel parameters [17]–[21]. Interpreting the mismatch between

measured and predicted channel parameters thus intuitively requires identification of potential sources of uncertainties and errors. The factors that affect the fidelity of channel parameters derived from RT tools can be broadly classified into three groups.

1) The inputs which encompasses the digital map, constitutive parameters of materials and antenna models.
2) The modeling of the interaction mechanisms such as reflection, diffraction, transmission, diffuse scattering and attenuation by vegetation.
3) The computation complexity reduction techniques that aim to keep the simulation time within reasonable limits. These include limiting the order of interaction mechanisms and in particular diffraction, map simplification and acceleration techniques [22]–[24].

Several works in the literature have reviewed various aspects of RT channel modeling. In [3], a review of acceleration techniques and propagation models used in academic and commercial RT is presented. In addition, the authors highlight novel applications of RT in fifth generation (5G) and beyond communication systems as well as calibration of RT simulators. In [10], a comprehensive review of propagation models, basic algorithms and acceleration techniques in RT is presented. The factors affecting the accuracy of RT are also briefly outlined and in particular digital maps, however, no quantitative results were presented in regards to the achieved accuracy in the literature. In [7], a review of the state-of-the-art RT techniques is presented with a focus on applications in small cells and indoor scenarios. The authors highlight the role of propagation models and in particular diffuse scattering in RT channel modeling as well as the need for accurate environment modeling.

In this article, a review of the achieved accuracy of RT radio prediction in outdoor scenarios for the sub-6 GHz frequency band is presented. Although recent research efforts in RT have mainly focused on mm-wave and terahertz frequencies, the sub-6 GHz band remains vital for legacy cellular systems and 5G frequency range 1 (FR1). Moreover, due to the frequency dependency of factors such as material electrical parameters and propagation phenomena models, research findings in one band are not directly transferable to a different frequency band thus a need to carry out analysis on a per band basis. It is worthwhile to highlight that even for the same frequency band, comparing different RT tools is not feasible due to differences in theoretical models implemented, computation complexity reduction techniques employed, diversity of scenarios under study and channel sounding equipment used for validation measurements. Therefore, this work aims at highlighting quantitatively the achieved accuracy for each study taken and factors therein that could have had an impact on the achieved accuracy. The main contribution of this article lie in the following.

1) A comprehensive survey of the achieved accuracy of path loss in the sub-6 GHz frequency band for outdoor deployment scenarios is presented.
2) A review of the accuracy of digital maps from cyberspace is also presented as these are some of the main sources of environment information in RT simulations, however, this is often not comprehensively highlighted in RT literature.
3) A review of representative material parameters used for RT outdoor scenario simulations in the literature at sub-6 GHz and their impact on channel prediction is presented.
4) Simulation results are presented for urban microcell (UMi) and urban macrocell (UMa) scenarios to highlight the impact of constitutive material parameter variation on the predicted path loss as this is the degree of freedom used in the calibration of RT tools.

The rest of the paper is organized as follows. Section II outlines the accuracy of the digital maps commonly used in RT and material parameters used, in Section III, a review of interaction mechanisms and their impact on channel predictions is presented. Section IV presents simulations to highlight the observations made in the literature and finally Section V concludes the paper.

II. SIMULATION INPUTS

In RT two main paradigms are adopted for the generation of site specific channel models: a) ray launching and b) the method of images. In the former approach, rays from the source are launched with uniform angular separation, traced in the scenario and the received field is then calculated at defined reception points [10], [22], [25]. The attractive features of this approach is relatively faster computation time compared with the method of images but it suffers from lower accuracy especially with an increase in the distance from the source due to spreading out of the rays. This lower accuracy stems from a lower number of rays received as the distance is increased assuming a fixed reception point size. In the latter approach, the trajectory of a ray is determined by first defining image points of the transmitter or alternatively the image point of the receiver. The interaction point is then obtained from the intersection of the line segment joining the transmitter to the receiver image point and the object defined in the environment database [10], [22]. Although the method of images achieves a higher prediction accuracy than the ray launching approach, it suffers from high computational complexity especially for large environmental databases e.g., outdoor simulations.

The process of generating a site specific channel model using RT is illustrated in Fig. 1. The RT engine can either be based on the ray launching or method of images and in some cases a hybrid of the two paradigms [22]. The interaction mechanisms implementation follows propagation theory, however, variation across different RT tools occurs due to different methods of modeling the same phenomena for example diffraction and diffuse scattering. Other variations occurs in the antenna models, sources of digital maps and material library used.

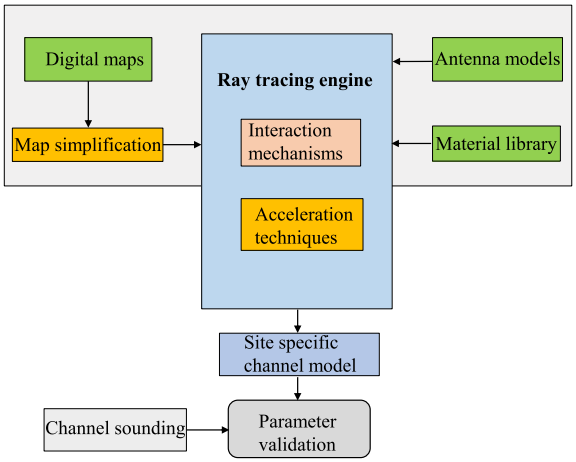

FIGURE 1. An overview of site specific channel model generation using RT.

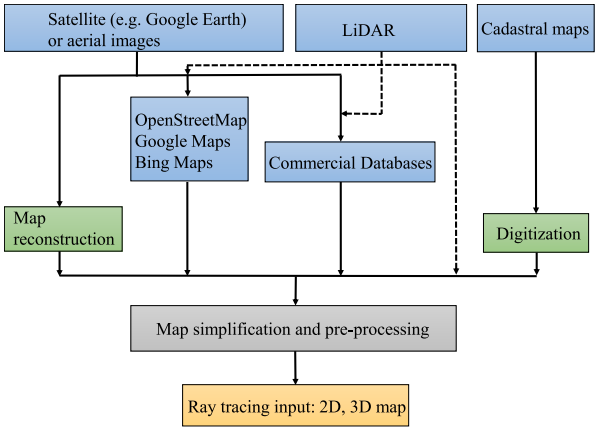

FIGURE 2. Digital map acquisition and pre-processing for outdoor RT simulations.

A. DIGITAL MAPS

1) SOURCES OF DIGITAL MAPS

Site specific propagation prediction using geometrical optics requires a description of the propagation scenario usually in the form of digital maps [26]. Some of the sources of environmental databases used in RT simulations in the literature include:

1) Commercial databases [27], where different map providers construct the map based on satellite or aerial images, local surveys or using point clouds obtained using light detection and ranging (LiDAR) [28], [29]. LiDAR based point clouds have also been used by some researchers to construct localized maps. However, due to a significant effort required to collect and process the point clouds, the geographical span is usually limited to e.g., campus, indoor [30] or outdoor scenarios of a few kilometers [12].
2) Cadastral or city maps [26], [31]–[36] from local authorities which are then digitized for use in RT simulations.
3) Maps reconstructed from satellite or aerial images and in particular images from Google Earth (GE) [37]–[42], where technological advancements in the field of photogrammetry and machine learning have particularly accelerated this approach.
4) Maps from cyberspace e.g., OpenStreetMap (OSM), Google Maps (GM) and Bing Maps.

An illustration of the digital map acquisition process is shown in Fig. 2. A pre-processing or map simplification stage is often employed prior to the input of RT tools to reduce computational complexity that may arise from the high details in digital maps [23], [43], [44]. The pre-processed digital maps are then used in RT tools as raster or vector formats and in some cases a hybrid of both formats is employed [45]. In the raster format, map features are stored in the form of pixels whereas the vector format stores information in the form of points, lines and polygons. The raster format suffers the penalty of higher storage requirement since higher resolution maps require more pixels to represent map features [46]. The vector format is most often preferred in RT since the description of map features as lines or polygons intuitively simplifies the determination of the reflection plane for instance [31].

2) DEFINITION OF A DIGITAL MAP'S ACCURACY

The accuracy of digital maps can be viewed from two broad perspectives: a micro-level and a macro-level perspective. On a micro-level, the accuracy of a map can be defined as the extent to which features such as surface roughness of walls [47], buildings facades [48], street lamps and vehicles are captured or approximated. Due to the practical difficulty of obtaining such level of detail in outdoor scenarios, a method used in the literature to account for micro-level details is by employing a statistical distribution to randomly add scatterers in the map [49]. On a macro-level perspective, a digital map's accuracy can be evaluated for the following features: 1) building footprints [44], 2) rooftops, 3) building edges and vertices, 4) horizontal positional accuracy, 5) vertical positional accuracy, and 6) the location of the antennas [50], [51].

3) ACCURACY OF MAPS FROM CYBERSPACE

The providers of maps in cyberspace do not publish the accuracy of their maps which makes it difficult to assess the impact of these maps on RT channel predictions. Nonetheless, several research groups have undertaken localized assessment of the positional accuracy of GE and OSM as outlined in Table 1. The ground truth or reference maps used for the assessments were based on Global Positioning System (GPS) reference points, cadastral maps or local surveys for the different locations considered. The use of cadastral maps as the source of ground truth can be seen to have a lower accuracy compared to GPS points since the cadastral maps also suffers from a limited accuracy. Indeed, the root mean squared error (RMSE) of the horizontal position accuracy of GE for instance was

TABLE 1. Accuracy of sources of digital maps.

Map	Evaluation Method	Location	Positional Accuracy (m)		Reference
			Horizontal	Vertical	
GE	GPS	Khartoum State, Sudan	RMSE: 1.80	RMSE: 1.73	[52]
GE	GPS Cadastral map[1]	Rome, Italy	RMSE: 0.45 RMSE: 1.45	- -	[53]
GE	Cadastral map[2]	Tamaulipas, Mexico	mean error: 4.1 STD: 2.9 RMSE: 5	- - -	[55]
GE	GPS	Montreal, Canada	RMSE: 1.08	-	[54]
OSM	Local survey[3]	Makah, Saudi Arabia	mean error: 3.35 RMSE: 1.57[4]	- -	[56]
OSM	Authoritative map[5]	Munich, Germany	mean error: 4.13 STD: 1.71	- -	[57]

[1] Italian cadastral mapping system.
[2] Mexican National Institute for Geography and Statistics.
[3] Topcon GTS710 Total Station and four GPS control points in the campus of UMM El-Qura university.
[4] The mean error and RMSE were 6.89 m and 4.82 m, respectively before the application of a two-dimensional (2D) affine transformation method.
[5] German Authority Topographic-Cartographic Information System.

observed to be below 2 m for GPS points in three different cities spread across three continents [52]–[54]. Although, these independent assessments provide a perspective of the accuracy of maps from cyberspace, it is worthwhile to highlight that maps from cyberspace are constantly updated. As such, differences in the accuracy could occur even for short time intervals as observed in [52], where the RMSE of the horizontal position accuracy of GE changed by 1.83 m in a span of two consecutive months.

4) IMPACT OF DIGITAL MAPS ACCURACY ON THE PREDICTED PATH LOSS

In [34], the impact of the digital map accuracy on the predicted path loss was evaluated by introducing random displacements of building walls of 0.5 m, 1 m, 2 m, and 3 m to the original map. When the original map was used, the predicted path loss with respect to the measurements had a mean error and RMSE of 0.7 dB and 3.5 dB, respectively. As the displacement of the building walls was introduced from 0.5 m, 1 m, 2 m, and then to 3 m, the mean error and RMSE of the predicted path loss were 1.1 dB, 0.5 dB, 0.9 dB, −2 dB, and 3.7 dB, 3.9 dB, 4.6 dB, 8.7 dB, respectively. Missing features in the original database were also observed to cause a mismatch of the predicted power at some sections of the receiver's route as these points had a relatively high RMSE of up to approximately 15 dB.

In [33], three types of maps: a cadastre map, a city map, and a 1:25000 map were digitized and stored in vector format. The cadastre map was digitized using a hand digitizer. The predicted path loss with respect to measurement using this map had a mean error and a standard deviation (STD) of 4.7 dB and 6.6 dB, respectively. The city map was digitized in a similar way and the predicted path loss observed to have a mean error and a STD of 10.3 dB and 9.2 dB, respectively. The 1:25000 map was in an electronic format thus automatic recognition algorithms were used to identify map features, where the identified errors were corrected manually. Using this map the predicted path loss was observed to have a mean error and a STD of −17.6 dB and 6.6 dB, respectively.

The cadastre map was then used to investigate the impact of random errors on the predicted path loss. Random errors with a STD of 0.5 m, 1 m, 1.5 m and 2 m in the building size and the location of the vertices were then artificially introduced. Path loss prediction was then performed using the erroneous maps and compared to the reference map without the artificial errors, which had a prediction accuracy of 0.2 dB and 7.4 dB in mean error and STD, respectively in comparison to measurements. As the STD of the random errors was increased from 0.5 m, 1 m, 1.5 m, and then to 2 m in the building size and vertices the probability of having a STD of the predicted path loss of less than 5 dB with respect to the reference prediction was then evaluated. The obtained probability was 99 %, 93 %, 88 %, 65 %, and 92 %, 32 %, 11 %, 3 % for the building size and vertices, respectively. The higher impact on the predicted path loss due to errors on building vertices compared to building size errors was attributed to the fact that the building vertices altered the street canyon effect which was the dominant mode of propagation for this particular scenario.

B. ELECTROMAGNETIC PROPERTIES OF MATERIALS

The constitutive material parameters, i.e., the electrical permittivity (ϵ), the magnetic permeability (μ), and the conductivity (σ) are fundamental for attaining realistic channel predictions in RT [3]. Indeed, the solution of Maxwell's equations for an electromagnetic wave at the boundary of different media is well known to depend on the constitutive parameters. This affects the amplitude and phase characteristics of the propagating wave and thus ultimately determines the contribution of individual multi-path components to the channel impulse response (CIR) for a particular propagation scenario.

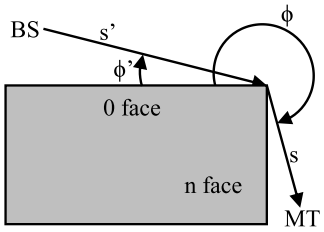

FIGURE 3. Diffraction on a corner modeled as a wedge.

1) MATERIAL PROPERTIES IN RAY TRACING

The impact of material properties on the RT prediction accuracy is dependent on the dominant propagation mode in a particular scenario. The line-of-sight (LoS) component, which is modeled using the Friss equation [58] has no dependence on constitutive material parameters. Consequently, in scenarios where the LoS is the dominant component, material properties have a minimal impact on the prediction accuracy. Diffuse scattering modeling in the RT literature is most often carried out using the effective roughness model proposed in [59]. This model is not based on Maxwell's equations, however, it solves the problem of accounting for the diffuse component power which is difficult to compute deterministically due to a lack of micro-level accuracy in the digital map. The effective roughness model has no material property dependence and hence the predicted diffuse scattered field will not have a dependence on the material property as well. Attenuation by vegetation is also modeled using empirical models e.g., the Weissberger, Single-tree and Torrico-Lang models [20], which have no dependence on material properties.

The significance of material properties in RT simulations can be demonstrated from the Fresnel's equations for the calculation of the reflection and transmission coefficient [3], [60], as well as the diffraction coefficient formula using the uniform theory of diffraction (UTD) for a finite conducting wedge which is widely adopted in several RT tools [49], [61]–[63]. For the sake of illustration purposes, these classical equations are included here.

Assuming a smooth reflection surface, the reflection coefficient Γ, for the perpendicularly ($\perp$) and parallel ($\parallel$) polarized wave at the boundary of media 1 and 2 can be obtained using Fresnel's equations as [64]:

$$\begin{aligned}\Gamma_{\perp} &= \frac{E^r_{\perp}}{E^i_{\perp}} = \frac{\eta_2 \cos\theta_i - \eta_1 \cos\theta_t}{\eta_2 \cos\theta_i + \eta_1 \cos\theta_t} \\ \Gamma_{\parallel} &= \frac{E^r_{\parallel}}{E^i_{\parallel}} = \frac{\eta_2 \cos\theta_t - \eta_1 \cos\theta_i}{\eta_2 \cos\theta_t + \eta_1 \cos\theta_i}\end{aligned} \tag{1}$$

where E^i, E^r, η, θ_i and θ_t are the incident electric field, reflected electric field, wave impedance, incident angle and transmission angle, respectively. The transmission coefficients for the perpendicularly and parallel polarized electric field can be obtained as [60]:

$$\begin{aligned}T_{\perp} &= \frac{E^t_{\perp}}{E^i_{\perp}} = \frac{2\eta_2 \cos\theta_i}{\eta_2 \cos\theta_i + \eta_1 \cos\theta_t} \\ T_{\parallel} &= \frac{E^t_{\parallel}}{E^i_{\parallel}} = \frac{2\eta_2 \cos\theta_t}{\eta_1 \cos\theta_t + \eta_2 \cos\theta_i}\end{aligned} \tag{2}$$

where E^t is the transmitted electric field. The material constitutive parameters in this case determine the wave impedance η and the transmission angle θ_t as:

$$\begin{aligned}\eta &= \sqrt{\frac{j\omega\mu}{\sigma + j\omega\epsilon}} \\ \cos\theta_t &= \sqrt{1 - \left(\frac{k_1}{k_2}\right)^2 (\sin\theta_i)^2}\end{aligned} \tag{3}$$

where ω and k are the angular frequency and the wave number for the f-th frequency, respectively and are defined as:

$$\begin{aligned}\omega &= 2\pi f \\ k &= \omega\sqrt{\mu\epsilon - \frac{j\mu\sigma}{\omega}}\end{aligned} \tag{4}$$

The impact of material parameters on the diffracted field in RT simulations depends on the diffraction model employed. Due to the significant computation complexity involved in calculating the diffracted field, simpler and less accurate models like the Berg's recursive model are often employed in RT tools, whereby the material properties in such a case do not affect the contribution of the diffracted field to the CIR [49], [65]. However, for a more accurate prediction of the diffracted field the UTD for a finite conducting wedge [66] is often used in RT simulations. However, this model requires a definition of the material constitutive parameters as outlined below. Consider a diffraction point as shown in Fig. 3, which can for instance be a building corner at a street intersection, the diffraction coefficient $D^{\perp}_{\parallel}$ can be obtained as [66]:

$$\begin{aligned}D^{\perp}_{\parallel} = {} & \frac{-e^{-j\pi/4}}{2n\sqrt{2\pi k}} \\ & \times \left\{ \cot\left(\frac{\pi + (\phi - \phi')}{2n}\right) \cdot F\left(kLa^{+}(\phi - \phi')\right) \right. \\ & + \cot\left(\frac{\pi - (\phi - \phi')}{2n}\right) \cdot F\left(kLa^{-}(\phi - \phi')\right) \\ & + \Gamma^{\perp}_{\parallel,0} \cdot \cot\left(\frac{\pi - (\phi + \phi')}{2n}\right) \cdot F\left(kLa^{-}(\phi + \phi')\right) \\ & + \Gamma^{\perp}_{\parallel,n} \cdot \cot\left(\frac{\pi + (\phi + \phi')}{2n}\right) \\ & \left. \times F\left(kLa^{+}(\phi + \phi')\right) \right\}\end{aligned} \tag{5}$$

TABLE 2. Material properties used in RT simulations at sub-6 GHz for outdoor scenarios.

Scenario	Frequency (GHz)	Material[1]	Conductivity (σ) S/m	Relative Permittivity (ϵ_r)	Reference
Urban	2 5.2	concrete (dry)[2]	-	$5 - j0.1$	[18]
Urban	0.85 1.9	uniform	0.02	5	[51]
Urban	2.154	uniform	0.01	5	[27]
Urban	0.9 2	uniform	0.005	15	[67]
Urban	1.823	uniform	0.005	5	[34], [35]
Urban	0.9 1.9	uniform	-	6	[68]
Urban	1.89	uniform	0.0001	5	[32], [33]
Urban	0.91	concrete	0.2	7	[69]
Urban	1.87	concrete	0.01	4	[70]
Urban	0.6	uniform	1	15	[62]
Urban	1.956 2.1119	uniform	2	15	[61]
Urban	0.91	uniform	0.2	7	[71]
Urban	0.9 1.5	uniform	7	15	[72]
Campus	1.823	sandstone (dry sand) ground	0.001 0.01	3.4 10	[73]
Campus	1.87	buildings ground	0.05 0.1	5.3 15	[74]
Campus	3.8	brick concrete	0.01 0.2	4.4 8.5	[75]

[1] The materials are assumed in most cases to be non-magnetic thus the permeability of free space is used [76].
[2] The streets are also assigned the same material parameters with a surface roughness of 1 mm.

where ϕ', ϕ are the angles of incidence and diffraction, respectively. $F(x)$ is a Fresnel's integral which is defined as

$$F(x) = 2j\sqrt{(x)}e^{jx}\int_{\sqrt{(x)}}^{\infty} e^{-j\tau^2}d\tau \tag{6}$$

L is defined as

$$L = \frac{ss'}{s+s'} \tag{7}$$

where n is the wedge factor, s' and s are the distances from the source to the diffracting wedge and from the wedge to the receiver, respectively. $a^{\pm}$ is defined as

$$a^{\pm}\left(\phi \pm \phi'\right) = 2\cos^2\left(\frac{2n\pi N^{\pm} - \left(\phi \pm \phi'\right)}{2}\right) \tag{8}$$

Finally, $N^{\pm}$ are the integers which closely satisfy the following equations

$$\begin{aligned} 2\pi nN^{+} - \left(\phi \pm \phi'\right) &= \pi \\ 2\pi nN^{-} - \left(\phi \pm \phi'\right) &= -\pi \end{aligned} \tag{9}$$

Knowledge of the material properties is thus critical for accurate modeling of diffraction since the calculation of the diffraction coefficient depends on the wave number k defined in (4) as well as the reflection coefficients $\Gamma^{\perp}_{\parallel,0}$ and $\Gamma^{\perp}_{\parallel,n}$ for the 0-th and n-th face of the wedge, respectively defined in (1), which are in turn dependent on the constitutive parameters of the materials in a particular propagation scenario.

2) CONSTITUTIVE PARAMETERS USED IN RAY TRACING TOOLS

Table 2 shows different material parameter values for RT simulations in the literature for outdoor scenarios in the sub-6 GHz frequency range. As can be observed, a common approach used in most RT simulations is to assign effective material parameters [27], [32]–[35], [51], [67], [68] or using one or several representative materials for the entire propagation scenario [18], [69], [70], [73], [75]. This approach is rather scenario specific and thus quite difficult to compare different RT simulations even in cases where the scenario and frequency settings are similar as can be seen in Table 2 for the references [32]–[35], [51]. In these cases, the relative permittivity used is identical but the conductivity varies by two orders of magnitude. The differences are brought about most likely by material parameter tuning which was done in [32]–[35] whereas it was not been carried out in [51].

The conductivity of concrete for the works presented in Table 2 for instance does not show any trend with an increase in frequency. This is in contradiction to the International Telecommunication Union (ITU) model in Fig. 4, where the conductivity of concrete is observed to increase with frequency [76]. This is also most likely due to material parameter tuning in the RT simulations. On the other hand, relative permittivity does not show a specific trend with frequency as per the ITU findings [76]. Similarly, in [77], no specific frequency trend for the relative permittivity can be observed for the different materials presented therein, with each material exhibiting a different behavior with frequency.

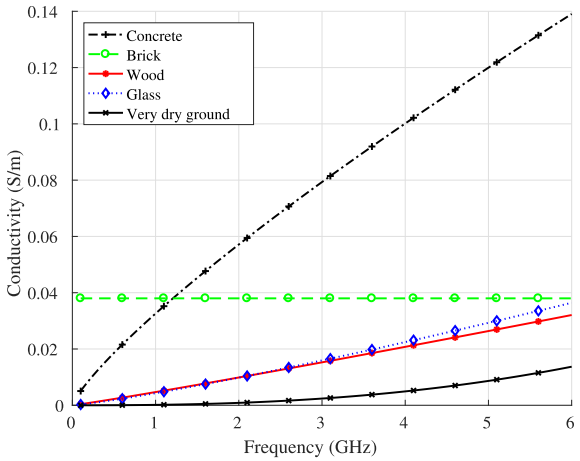

FIGURE 4. Frequency dependency of conductivity for selected materials at sub-6 GHz based on the recommendation in [76].

Defining the constitutive parameters of individual materials in a propagation scenario, particularly outdoor scenarios, is a daunting task due to the following reasons:

1) Materials in a particular scenario are very diverse and not known *a priori*.
2) The constitutive parameters exhibit a frequency dependence as well as variation with temperature and humidity [64], [76]–[79]. This was demonstrated in [74], where a variation of humidity from 0% to 15% resulted in a change of the power of some multi-path components by up to 6 dB.
3) Common building materials are heterogeneous, where for the same material type e.g., glass, the chemical composition differs depending on the manufacturing process [78]–[80].
4) Presence of air gaps and moisture in building materials like brick could cause a variation of constitutive parameters [77], [79].
5) Few extensive measurements reported in the literature for wide frequency range and material variety [76], [77].

These reasons have thus led to the uniform material parameters approach commonly employed in most RT simulations [51], [81]. Calibration or tuning of the material properties is in some cases performed to attain effective material parameters which attain the best match with measurements [34], [82], [83].

3) IMPACT OF MATERIAL PARAMETERS ON PATH LOSS PREDICTION

The dependence of the reflection, transmission and diffraction coefficient on the material properties in turn has a direct influence on the predicted channel parameters e.g., the path loss [32], [34]. In [34], with the assumption of uniform material properties for the entire propagation scenario, the conductivity was varied from 10^{-12} S/m to 10 S/m, where for values between 10^{-12} S/m and 0.0005 S/m, the change of the RMSE of the predicted path loss was 0.7 dB. On the other hand, the authors demonstrated that high conductivity of the walls (10 S/m) resulted in an under estimation of the path loss with a mean error and RMSE of 17.8 dB and 20.8 dB, respectively. A conductivity of 0.005 S/m was observed to attain the lowest mean error and RMSE of 0.7 dB and 3.5 dB, respectively in comparison to measured path loss. The impact of the relative permittivity on the path loss was investigated by using four different values 3, 3.5, 5, and 7. The mean error and the RMSE of the path loss in comparison to measurement were −3.3 dB, −1 dB, 0.7 dB, 3.3 dB, and 6.7 dB, 4 dB, 3.5 dB, 4.6 dB, respectively for the four values of permittivity. The deep non-line-of-sight (NLoS) regions were observed to be most sensitive to the change of the relative permittivity of the walls. Although the mean received power increased by approximately by 3 dBm for each increase in the relative permittivity from 3, 3.5, 5, and 7, this relationship was not found to be conclusive due to presence of sudden peaks and drops in the received power along the receiver's route.

In [32], the impact of the relative permittivity on the reflection coefficient was evaluated by fixing the order of reflection to nine, the order of diffraction to one and the conductivity to 10^{-4} S/m. The mean error and STD of the predicted path loss in relation to measurements were then evaluated for relative permittivity values 2, 4, 5, 6, 8, and 10. The STD was found to be between 7.1 dB and 8.1 dB. However, the mean error increased progressively from −8.5 dB to 5.4 dB for an increase in the relative permittivity from 2 to 10 with the lowest mean error of −0.2 dB obtained for a relative permittivity of 5. In [61], when the relative permittivity was fixed to 15, no significant effect was observed for a variation of conductivity from 0 S/m to 7 S/m for the LoS scenario, whereas for the NLoS scenario the impact on the path loss was insignificant when conductivity was varied from 2 S/m to 7 S/m.

III. INTERACTION MECHANISMS

In RT, the concepts of ray optics are used to solve Maxwell's equations asymptotically in the high frequency regime [84]. In comparison to full-wave methods of solving Maxwell's equation, RT achieves accurate results within reasonable computation time when the propagation scenario is several orders greater than the wavelength of the electromagnetic wave [85], [86]. Depending on the electrical and geometrical characteristics of the objects in the digital map, a ray might undergo reflection, diffraction, penetration, diffuse scattering or attenuation by vegetation. Thus the mode of interaction of the ray with the propagation scenario hinges upon an accurate geometrical and material property description in the environment model.

The computational complexity of RT tools has generally been observed to increase with the order of interaction mechanisms. However, with higher order interactions, the gains in terms of prediction accuracy are often marginal

but nonetheless incurring significant computational overhead [23]. Two main methods are employed in RT studies to address the computational complexity resulting from using a high order of interaction mechanisms. The first approach entails neglecting rays whose power contribution is below a certain threshold [23] and the second approach is where the sufficient order of reflections are determined heuristically [34].

A. REFLECTION

Reflection in most RT tools in the literature is mainly modeled in using Fresnel's equations (1). However, due to a lack of material constitutive parameters, some authors resort to using a constant reflection loss for each reflected ray [33]. In [26], a reflection loss of 12 dB was used for all building surfaces, whereas in [31] a constant reflection loss of 15 dB is used and in [87] a reflection loss of 6 dB considered. The latter approach is often an over simplification of the reflection mechanism since as illustrated in [62] and (1), the magnitude and phase of the reflection coefficient are not only dependent on the constitutive parameters of materials but also on the angle of incidence. The use of Fresnel's equations is thus generally preferred in most RT studies where even with limited material constitutive parameters, effective or uniform material parameters are used for the entire propagation scenario as shown in Table 2.

In [34], an investigation of the sufficient order of specular reflections was carried out. In the LoS regions, minute differences in the path loss were observed for three, five, seven and nine orders of reflections. However, in the deep NLoS regions, higher order reflections were observed to be crucial for accurate prediction of the path loss. In comparison to measurements, the simulation with nine orders of reflection had a mean error and RMSE of 0.9 dB and 3.5 dB, respectively, whereas with three orders of reflection the mean error and RMSE were -2.3 dB and 7.2 dB, respectively. In [88], it was observed that increasing the number of specular reflections from 10 to 100 only had an improvement of less than 1 dB in prediction accuracy of path loss. Generally, three orders of reflections are observed in most RT studies [20], [51], [75], [89], [90].

B. DIFFRACTION

In [34], the effect of diffraction modeling on RT predictions was demonstrated where with seven orders of reflection and neglecting diffraction resulted in a mean error and a RMSE of -12.5 dB and 28 dB, respectively. The inclusion of one order of diffraction dramatically improved the path loss prediction, where a mean error of 0.7 dB and a RMSE of 3.5 dB were attained. This was attributed to the fact that for the scenario under consideration, omitting diffraction resulted in no predicted propagation paths for the NLoS regions. Subsequent increase in the diffraction order showed marginal prediction improvement, where for both the mean error and the RMSE of the predicted path loss, the change was less than 1 dB. In [91], diffraction modeling in combination with a digital map was shown to result in a good agreement with the measured path loss, however, as the path loss increased the prediction accuracy reduced. To improve the prediction accuracy, it was suggested that additional propagation mechanisms like scattering need to be included in the RT simulation. In [32], single diffraction per path by building corners is investigated by comparing three different diffraction coefficients: the perfectly absorbing wedge, the UTD and the heuristic extension of the UTD. In comparison to measurements, the highest mean error and STD obtained were 2.7 dB and 7.3 dB, respectively. The three diffraction coefficients were observed to give equally good predictions bearing in mind that the measurement data had a degree of uncertainty since a STD of 3 dB was observed for repeat measurements. Double diffraction was then investigated and the highest mean error and STD were found to be 5.2 dB and 7.3 dB, respectively.

C. DIFFUSE SCATTERING

When surfaces are not smooth, the interaction of an electromagnetic wave and the surface results in dispersion of energy in stochastic directions, where this phenomena is commonly defined as diffuse scattering [19], [59], [92]. The classification of surfaces as smooth or rough is determined heuristically in RT e.g., using the Fraunhofer criterion which introduces a frequency dependence [92]. Due to the law of conservation of energy, diffuse scattering causes a reduction of the reflected power. Therefore, the Fresnel's reflection coefficient is usually scaled to account for the diffuse component of the signal power [19]. The significance of diffuse scattering in outdoor propagation was demonstrated in a measurement campaign carried out in [21]. The authors considered two types of buildings; typical rural and office buildings. The ratio of the diffuse scattered power to the total back scattered power was found to be approximately 30% and 50%, for the rural and office building, respectively, where the higher contribution of the diffuse component in the office building was attributed to its facade's complex metallic structure.

In [51], the predicted path loss was observed to improve by the inclusion of diffuse scattering and over the roof top propagation especially in the deep NLoS regions. In comparison to measurement, inclusion of diffuse scattering improved the path loss prediction where a mean error, STD and RMSE of 1.3 dB, 7.3 dB and 7.4 dB, respectively were attained compared to -9 dB, 13.3 dB and 9.8 dB, respectively for the prediction without diffuse scattering in the simulation. In [75], the inclusion of diffuse scattering was shown to reduce the mean prediction error of path loss by 5.7 dB. Moreover, the delay spread prediction was also shown to improve with the inclusion of diffuse scattering in the RT simulation. In [20], a combination of diffuse scattering and attenuation by vegetation was shown to reduce the RMSE of the predicted path loss by approximately 4 dB.

In addition to improving the prediction accuracy of path loss, diffuse scattering in RT enables a better prediction of delay and angle spreads since it accounts for paths from a wider solid angle compared to reflection and diffraction [27]. Indeed, it was demonstrated in [27] that simulations with diffuse scattering achieved a closer match to the measured angle and delay spread along the propagation routes, whereas simulations with no diffuse scattering resulted in an underestimation of the two channel parameters.

IV. SIMULATIONS WITH THE METIS RAY TRACING TOOL

A summary of the achieved prediction accuracy of path loss for various RT tools in the literature is outlined in Table 3. It can be seen RT achieves reasonably accurate predictions of path loss considering the variety of scenarios and interaction mechanisms considered in the references therein. In this Section, path loss will be the channel parameter considered for the evaluation of the impact of parameter variation in the simulations carried out herein for the following reasons:

1) Path loss is more robust to inaccuracies in digital maps and placement errors of antennas in comparison to delay and angle spread.
2) Path loss is always the basic requirement for network planning in legacy communication systems as well as the 5G cellular system.

Nonetheless, delay spread remains an important parameter for orthogonal frequency division multiple (OFDM) access based systems as it determines the necessary guard band required to prevent detrimental effects of inter-symbol interference. On the other hand, angle spread is critical for multiple-input multiple-output (MIMO) systems since higher throughput relies on having several independent paths in the channel. As more accurate digital map are emerging and more double directional channel measurements are carried, these two channel parameters are gaining attention in the RT literature, however, the results are still not conclusive.

The METIS RT tool [49] is used to investigate the impact of the material parameter selection on the predicted path loss for two diffraction models, the UTD for a finite conducting wedge and the Berg's recursive model. Since the RT tool is already validated in [49] for a variety of scenarios: indoor, outdoor and vehicle to vehicle (V2V), the objective here is to highlight the observations for the literature reviewed in the preceding Sections rather than a validation of the RT tool itself. Two configurations i.e., the UMi and the UMa are considered for the "Madrid grid" which is composed of irregular building heights. The buildings are assumed to be made of concrete with a relative permittivity of 4.5 and a conductivity of 0.09 S/m. The value of conductivity is chosen for a frequency of 3.7 GHz based on the ITU recommended model [76] illustrated in Fig. 4. Similarly, the value of the relative permittivity of concrete is obtained from the literature to mimic the representative material property [96].

The base station (BS) location is fixed on the map and only the height is changed from 5 m for the UMi to 50 m for the UMa configuration. The mobile terminal (MT) height is

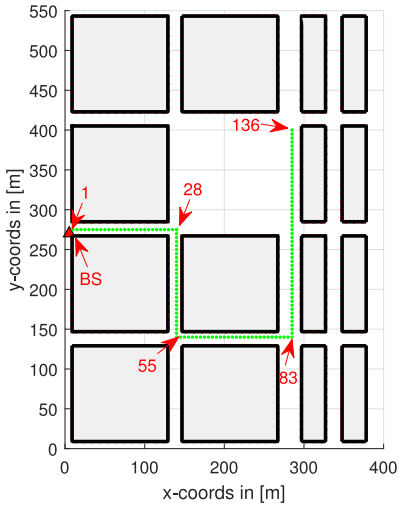

FIGURE 5. 2D Map of the Madrid grid illustrating the BS position indicated by the triangle and the MT route indicated by the dashed line.

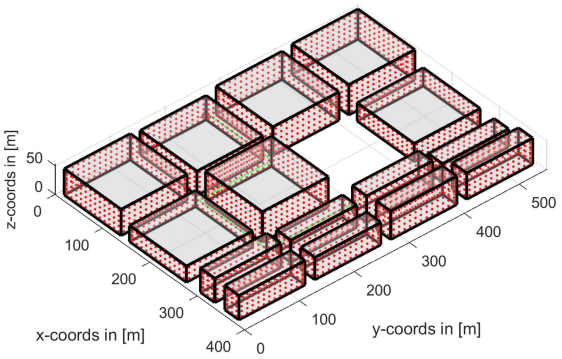

FIGURE 6. 3D Map of the Madrid scenario illustrating the tiles for diffuse scattering calculation and the irregular building heights.

2 m and its route is the same for both configurations, which is illustrated in Fig. 5. A total of 136 positions are considered, where the distance is increased uniformly by 5 m from the starting position. The route is selected such that there are regions in LoS (position 1 to 27 and 110 to 116), NLoS (position 28 to 55, 117 to 136) and deep NLoS conditions (position 55 to 83).

The scattering tile for the diffuse scattering calculation are set to 10×10 m and are uniformly distributed on the wall surface as shown in Fig. 6. In addition, surfaces are assumed to have a surface roughness with a STD of 0.001 m. The ratio of the specular to diffuse scattered power is 0.5. In these simulations, only one order of specular reflection and diffraction are considered.

Simulations are then carried out for conductivity values of 0.09 S/m, 7 S/m and 10^3 S/m are for a fixed relative permittivity of 4.5. Similarly, the simulations are run for different values of relative permittivity: 1, 4.5, 9, and 15 for a fixed conductivity value of 0.09 S/m. These values are selected based on the typical values used in the literature as outlined in Table 2. Two diffraction models are then considered for each simulation, the UTD for a finite

TABLE 3. Accuracy of path loss for outdoor scenarios at sub-6 GHz.

Scenario	Frequency (GHz)	LoS/NLoS	Mean Error (dB)	STD (dB)	RMSE (dB)	Reference
Campus	3.8	LoS, NLoS	-	-	4	[20]
Campus	3.8	LoS, NLoS	3.5	-	-	[75]
UMa	2 5.2	LoS, NLoS	1.3	2.8	-	[18]
UMa	0.85 1.9	LoS, NLoS	1.3	7.4	7.5	[51]
UMa, UMi	2.154	LoS, NLoS	−2.9 to 3.7	3.3 to 5.4	-	[27]
UMa	0.811 2.63	LoS, NLoS	-	-	11.4 13.6	[93]
UMa	0.947	LoS, NLoS	−2.6 to −0.4	6.2 to 8.3	-	[94]
UMa	0.85 1.9	-	2.1	7.5	-	[90]
UMa	1.8	LoS, NLoS	0.1	7.6	-	[45]
Urban, V2V	5.6	LoS NLoS	0.1 5.4	1.3 5.3	-	[89]
Urban, V2V	5.6	LoS NLoS	0.9 to 3.1 11.2 to 26.2	1.7 to 5.4 2.8 to 6	-	[14]
UMa	0.9 2	NLoS	−5.3 to 0.6	3.4 to 5.7		[67]
UMi UMa	0.9 1.9 0.9 1.9	LoS, NLoS	2.4 2.3 7.2 0.9	9.2 9.9 6.8 6.9	-	[68]
Urban, V2V	5.2	LoS, NLoS	0.8	2.8	-	[95]
UMi	1.89	LoS, NLoS	2.7	7.3	-	[32]
UMi	1.89	LoS, NLoS	0.2	7.4	-	[33]
UMi	1.823	LoS, NLoS	0.7	-	3.5	[34]
UMi	1.823	LoS, NLoS	1.1	3.7	3.7	[35]
UMa	0.89	-	1	5	-	[36]

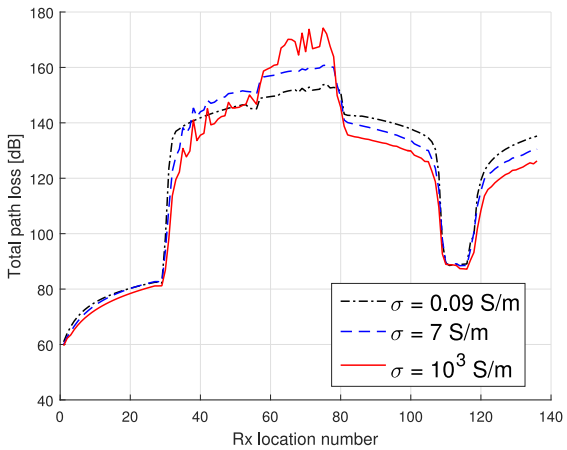

FIGURE 7. Path loss at different MT positions for $\sigma = 0.09$ S/m, 7 S/m, and 10^3 S/m for the UMi configuration. $\epsilon_r = 4.5$. Diffraction model: UTD.

conducting wedge [66] and the Berg's recursive model [65]. Random scattering objects are not included in the simulation. Although this is supported by the RT tool, the objective here is to identify the effect of material parameter variation on a map defined in the macro-level as outlined in Section II.

A. URBAN MICROCELLULAR SCENARIO

In the UMi scenario, propagation over the rooftop is disabled by default as both the BS and MT antennas are below the rooftop. The simulation with a relative permittivity of 4.5 and a conductivity of 0.09 S/m is used as the reference simulation.

1) CONDUCTIVITY VARIATION

The path loss can be observed to be less sensitive to conductivity variation in the LoS section of the route, positions 1 to 28 and 110 to 116, compared to the deep NLoS sections of the route as shown in Fig. 7 for the UTD diffraction model. This is due to the fact that in the LoS section, the LoS component is the most dominant propagation mechanism. As the conductivity is increased the path loss is observed to reduce since the power of the reflected paths increases. However, in the MT route from position 56 to 83, higher conductivity can be observed to cause an increase in the path loss. In this section of the MT route, the number of rays to the MT are approximately two times lower than of those in the preceding and successive NLoS sections. In addition, the dominant propagation mechanism is diffraction since as can be observed by the differences in Fig. 7 and Fig. 8, the choice of the diffraction model results in a significant difference in the path loss.

Apart from the lower number of rays reaching the MT, the higher predicted path loss with the UTD diffraction model in this section of the MT route compared to the Berg's recursive model is due to the fact that as the observation angle (ϕ in Fig. 3) increases and goes to the shadow region, the predicted power with the UTD model drops significantly as outlined in [97], [98].

2) RELATIVE PERMITTIVITY VARIATION

The variation of relative permittivity for the UMi configuration with the UTD diffraction model is shown in Fig. 9.

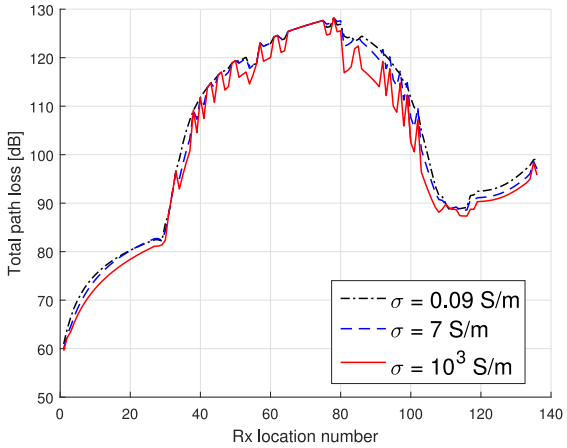

FIGURE 8. Path loss at different MT positions for $\sigma = 0.09$ S/m, 7 S/m, and 10^3 S/m for the UMi configuration. $\epsilon_r = 4.5$. Diffraction model: Berg's recursive model.

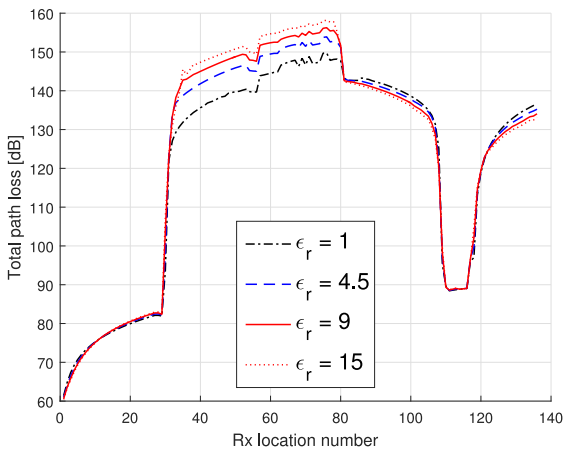

FIGURE 9. Path loss at different MT positions for $\epsilon_r = 1$, 4.5, 9, and 15 for the UMi configuration. $\sigma = 0.09$ S/m. Diffraction model: UTD.

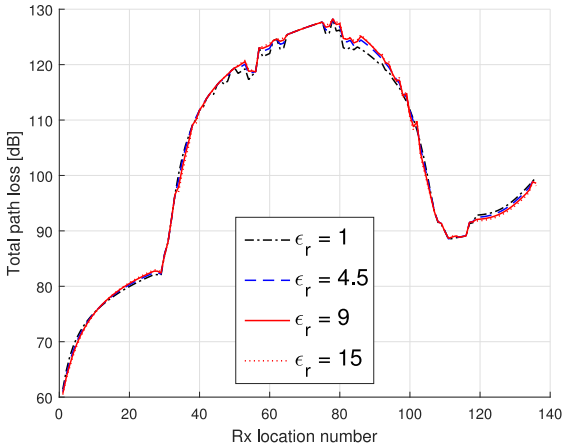

FIGURE 10. Path loss at different MT positions for $\epsilon_r = 1$, 4.5, 9, and 15 for the UMi configuration. $\sigma = 0.09$ S/m. Diffraction model: Berg's recursive model.

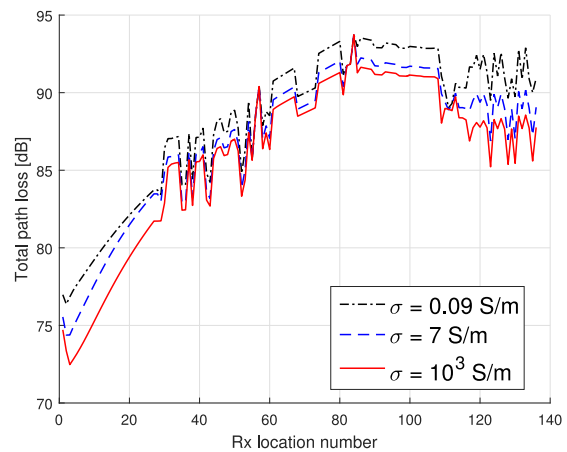

FIGURE 11. Path loss at different MT positions for $\sigma = 0.09$ S/m, 7 S/m and 10^3 S/m for the UMa configuration. $\epsilon_r = 4.5$. Diffraction model: UTD.

In the LoS section of the MT route path loss is shown to be less sensitive to the change in the relative permittivity, however, in the deep NLoS section of the route, an increase in the relative permittivity led to an increase in the path loss. The dominant propagation mechanism in this section of the MT route is diffraction. For the UTD diffraction model considered, the increase in the path loss with the increase in relative permittivity has been also observed in the literature [98], [99], where a relative permittivity of 3 caused approximately up to a 10 dB lower path loss compared to a relative permittivity of 8 in some observation angles. A similar phenomena can be observed in Fig. 9.

The effect of the change of relative permittivity on the path loss for the Berg's diffraction model is illustrated in Fig. 10. A low sensitivity of the path loss to the change in the relative permittivity can be observed in both the LoS and NLoS sections of the MT route.

B. URBAN MACROCELLULAR SCENARIO

In the UMa scenario, propagation over the rooftop is enabled as the BS antenna is above the rooftop. Indeed, this propagation mechanism has been observed in the literature to contribute significantly to the received signal power in NLoS scenarios in UMa setups [59]. The simulation with a relative permittivity of 4.5 and a conductivity of 0.09 S/m is used as the reference simulation.

1) CONDUCTIVITY VARIATION

An increase in the conductivity is observed to result in a higher received power for the UMa scenario for the UTD and Berg's recursive model in Fig. 11 and Fig. 12, respectively. However, the Berg's recursive model is shown to result in a higher path loss compared to the UTD model. This is because being a semi-empirical model, the Berg's model does not exploit the material constitutive parameters to attain finer prediction accuracy. A comparison of the two models intuitively shows that diffraction is the dominant propagation mechanism in the NLoS sections of the MT route as this is where significant differences occur for the choice of two different diffraction models.

These differences in the two models especially for the NLoS regions show the importance of having accurate material description in the environment model. The path loss in

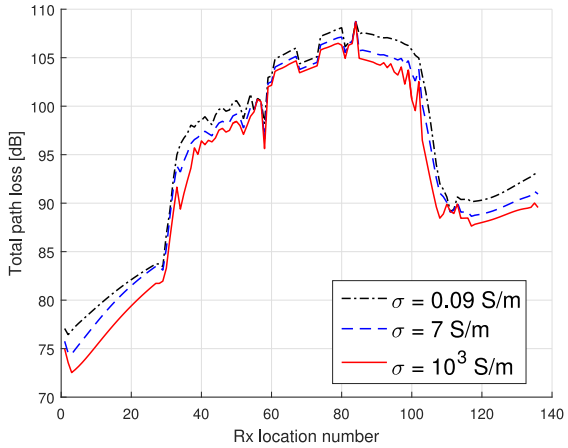

FIGURE 12. Path loss at different MT positions for $\sigma = 0.09$ S/m, 7 S/m and 10^3 S/m for the UMa configuration. $\epsilon_r = 4.5$. Diffraction model: Berg's recursive model.

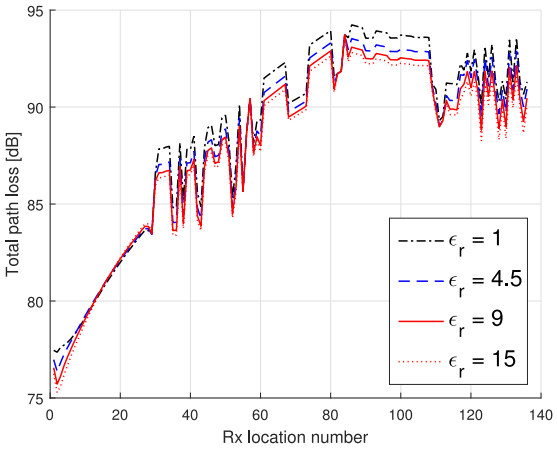

FIGURE 13. Path loss at different MT positions for $\epsilon_r = 1$, 4.5, 9, and 15 for the UMa configuration. $\sigma = 0.09$ S/m. Diffraction model: UTD.

the LoS section of the MT route (position 1 to 28) can also be observed to be more sensitive to the change in the conductivity compared to the UMi scenario in Fig. 7. This is caused by the reduced power contribution of the LoS component due to the ten times increase of the height of the BS. Intuitively, increasing the conductivity leads to an increase in the power of the reflected paths while the power of the LoS remains constant.

2) RELATIVE PERMITTIVITY VARIATION

The relative permittivity for the UTD diffraction model is illustrated in Fig. 13. In the LoS section of the route, a low sensitivity of the path loss due to a change in the relative permittivity is observed as was the case in the UMi configuration. The NLoS section of the MT route can be observed to be more sensitive to changes in the relative permittivity compared to the LoS section.

This is also observed in the Berg's recursive models as illustrated in Fig. 14. This is due to the fact that the BS is above the buildings surrounding this section of the MT route hence reflected paths from the building walls now

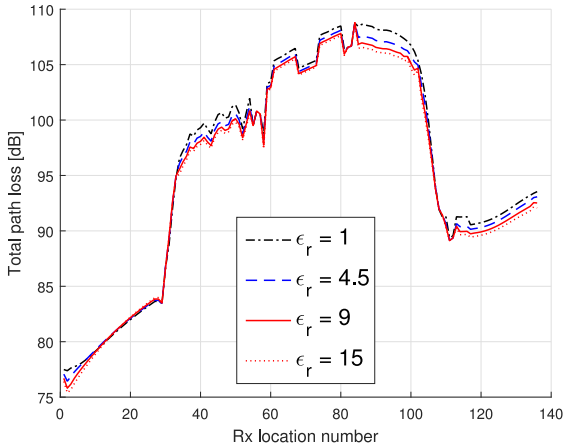

FIGURE 14. Path loss at different MT positions for $\epsilon_r = 1$, 4.5, 9, and 15 for the UMa configuration. $\sigma = 0.09$ S/m. Diffraction model: Berg's recursive model.

have a dominant contribution. In addition, paths from over the rooftop propagation are also included which reduces the total path loss. This is in contrast to the UMi scenario where diffraction was observed to be the dominant mechanism in the deep NLoS section (position 55 to 83).

V. CONCLUSION AND FUTURE OUTLOOK

In this article, a review of the achieved accuracy for path loss prediction in the literature for sub-6 GHz outdoor scenarios has been presented. RT has been shown to achieve reliable predictions with regard to path loss. An accurate description of the constitutive parameters is shown to be crucial especially for the NLoS regions where the predicted received power is most affected by the value of the reflection and diffraction coefficients. Attaining plausible prediction results nonetheless requires a high granularity in the analysis of the accuracy of the inputs, impact of acceleration techniques as well as models used and assumptions thereof for the different propagation mechanisms.

Due to the practical difficulties of performing channel measurements in diverse propagation scenarios, RT simulations have been proved useful especially in research on self-driving vehicles where many channel snapshots are required e.g., to capture the Doppler spectrum. This has led to novel RT simulation techniques e.g., dynamic RT [100], where dynamic scenarios can be simulated at significantly reduced computational time compared to conventional RT. Real time RT is further required in applications such as RT assisted beamforming, where beamforming weights are obtained from RT simulations [101].

Nonetheless, there are several open challenges in RT. Real time RT has been largely hampered by the computational complexity and research on dynamic RT is still in the early stages. Environment modeling also remains on a macro-level with micro-level details largely unaddressed. However, micro-level details are crucial as they can significantly impact diffuse scattering which would result in inaccurate prediction of channel parameters such as path

loss, angle and delay spread. In addition, material parameters remain scarce which leads to the use of effective material properties. More data on material properties across different frequency bands and the variation of the properties with external factors such as humidity is thus required improve the achievable prediction accuracy. Furthermore, sufficient validation measurements for different frequency bands and deployment scenarios are still lacking in the literature.

ACKNOWLEDGMENT

The authors would like to thank Dr. P. Kyösti for the fruitful discussion on map based channel modeling.

REFERENCES

[1] K. Guan *et al.*, "Scenario modules, ray-tracing simulations and analysis of millimetre wave and terahertz channels for smart rail mobility," *IET Microw. Antennas Propag.*, vol. 12, no. 4, pp. 501–508, Mar. 2018.

[2] K. Guan *et al.*, "Channel characterization for intra-wagon communication at 60 and 300 GHz bands," *IEEE Trans. Veh. Technol.*, vol. 68, no. 6, pp. 5193–5207, Jun. 2019.

[3] D. He, B. Ai, K. Guan, L. Wang, Z. Zhong, and T. Kürner, "The design and applications of high-performance ray-tracing simulation platform for 5G and beyond wireless communications: A tutorial," *IEEE Commun. Surveys Tuts.*, vol. 21, no. 1, pp. 10–27, 1st Quart., 2019.

[4] E. M. Vitucci *et al.*, "Tuning ray tracing for mm-Wave coverage prediction in outdoor urban scenarios," *Radio Sci.*, vol. 54, no. 11, pp. 1112–1128, 2019.

[5] J. W. McKown and R. L. Hamilton, "Ray tracing as a design tool for radio networks," *IEEE Netw.*, vol. 5, no. 6, pp. 27–30, Nov. 1991.

[6] A. Breglia, A. Capozzoli, C. Curcio, and A. Liseno, "Comparison of acceleration data structures for electromagnetic ray-tracing purposes on GPUs [EM programmer's notebook]," *IEEE Antennas Propag. Mag.*, vol. 57, no. 5, pp. 159–176, Oct. 2015.

[7] F. Fuschini, E. M. Vitucci, M. Barbiroli, G. Falciasecca, and V. Degli-Esposti, "Ray tracing propagation modeling for future small-cell and indoor applications: A review of current techniques," *Radio Sci.*, vol. 50, no. 6, pp. 469–485, 2015.

[8] J. S. Lu *et al.*, "A discrete environment-driven GPU-based ray launching algorithm," *IEEE Trans. Antennas Propag.*, vol. 67, no. 2, pp. 1180–1192, Feb. 2019.

[9] M. M. Taygur, I. O. Sukharevsky, and T. F. Eibert, "A bidirectional ray-tracing method for antenna coupling evaluation based on the reciprocity theorem," *IEEE Trans. Antennas Propag.*, vol. 66, no. 12, pp. 6654–6664, Dec. 2018.

[10] Z. Yun and M. F. Iskander, "Ray tracing for radio propagation modeling: Principles and applications," *IEEE Access*, vol. 3, pp. 1089–1100, 2015.

[11] W. Fan, I. Carton, P. Kyósti, and G. F. Pedersen, "Emulating ray-tracing channels in multiprobe anechoic chamber setups for virtual drive testing," *IEEE Trans. Antennas Propag.*, vol. 64, no. 2, pp. 730–739, Feb. 2016.

[12] J. Cao *et al.*, "Design and verification of a virtual drive test methodology for vehicular LTE-A applications," *IEEE Trans. Veh. Technol.*, vol. 67, no. 5, pp. 3791–3799, May 2018.

[13] L. Reichardt, J. Pontes, W. Wiesbeck, and T. Zwick, "Virtual drives in vehicular communication," *IEEE Veh. Technol. Mag.*, vol. 6, no. 2, pp. 54–62, Jun. 2011.

[14] T. Abbas, J. Nuckelt, T. Kürner, T. Zemen, C. F. Mecklenbräuker, and F. Tufvesson, "Simulation and measurement-based vehicle-to-vehicle channel characterization: Accuracy and constraint analysis," *IEEE Trans. Antennas Propag.*, vol. 63, no. 7, pp. 3208–3218, Jul. 2015.

[15] K. Guan *et al.*, "On the influence of scattering from traffic signs in vehicle-to-X communications," *IEEE Trans. Veh. Technol.*, vol. 65, no. 8, pp. 5835–5849, Aug. 2016.

[16] K. Schuler, D. Becker, and W. Wiesbeck, "Extraction of virtual scattering centers of vehicles by ray-tracing simulations," *IEEE Trans. Antennas Propag.*, vol. 56, no. 11, pp. 3543–3551, Nov. 2008.

[17] T. Rautiainen, G. Wolfle, and R. Hoppe, "Verifying path loss and delay spread predictions of a 3D ray tracing propagation model in urban environment," in *Proc. IEEE 56th Veh. Technol. Conf.*, vol. 4, 2002, pp. 2470–2474.

[18] T. Fugen, J. Maurer, T. Kayser, and W. Wiesbeck, "Capability of 3-D ray tracing for defining parameter sets for the specification of future mobile communications systems," *IEEE Trans. Antennas Propag.*, vol. 54, no. 11, pp. 3125–3137, Nov. 2006.

[19] V. Degli-Esposti, F. Fuschini, E. M. Vitucci, and G. Falciasecca, "Measurement and modelling of scattering from buildings," *IEEE Trans. Antennas Propag.*, vol. 55, no. 1, pp. 143–153, Jan. 2007.

[20] F. Mani and C. Oestges, "A ray based method to evaluate scattering by vegetation elements," *IEEE Trans. Antennas Propag.*, vol. 60, no. 8, pp. 4006–4009, Aug. 2012.

[21] E. M. Vitucci, F. Mani, V. Degli-Esposti, and C. Oestges, "Polarimetric properties of diffuse scattering from building walls: Experimental parameterization of a ray-tracing model," *IEEE Trans. Antennas Propag.*, vol. 60, no. 6, pp. 2961–2969, Jun. 2012.

[22] M. F. Iskander and Zhengqing Yun, "Propagation prediction models for wireless communication systems," *IEEE Trans. Microw. Theory Tech.*, vol. 50, no. 3, pp. 662–673, Mar. 2002.

[23] V. Degli-Esposti, F. Fuschini, E. M. Vitucci, and G. Falciasecca, "Speed-up techniques for ray tracing field prediction models," *IEEE Trans. Antennas Propag.*, vol. 57, no. 5, pp. 1469–1480, May 2009.

[24] S. Hussain and C. Brennan, "Efficient preprocessed ray tracing for 5G mobile transmitter scenarios in urban microcellular environments," *IEEE Trans. Antennas Propag.*, vol. 67, no. 5, pp. 3323–3333, May 2019.

[25] G. Durgin, N. Patwari, and T. S. Rappaport, "An advanced 3D ray launching method for wireless propagation prediction," in *Proc. IEEE 47th Veh. Technol. Conf.*, vol. 2, 1997, pp. 785–789.

[26] K. R. Schaubach and N. J. Davis, "Microcellular radio-channel propagation prediction," *IEEE Antennas Propag. Mag.*, vol. 36, no. 4, pp. 25–34, Aug. 1994.

[27] F. Fuschini, H. El-Sallabi, V. Degli-Esposti, L. Vuokko, D. Guiducci, and P. Vainikainen, "Analysis of multipath propagation in urban environment through multidimensional measurements and advanced ray tracing simulation," *IEEE Trans. Antennas Propag.*, vol. 56, no. 3, pp. 848–857, Mar. 2008.

[28] A. Boyko and T. Funkhouser, "Extracting roads from dense point clouds in large scale urban environment," *ISPRS J. Photogramm. Remote Sens.*, vol. 66, no. 6, pp. S2–S12, 2011.

[29] D. Lv, X. Ying, Y. Cui, J. Song, K. Qian, and M. Li, "Research on the technology of LIDAR data processing," in *Proc. 1st Int. Conf. Electron. Instrum. Inf. Syst. (EIIS)*, 2017, pp. 1–5.

[30] J. Järveläinen, K. Haneda, and A. Karttunen, "Indoor propagation channel simulations at 60 GHz using point cloud data," *IEEE Trans. Antennas Propag.*, vol. 64, no. 10, pp. 4457–4467, Oct. 2016.

[31] R. Grosskopf, "Prediction of urban propagation loss," *IEEE Trans. Antennas Propag.*, vol. 42, no. 5, pp. 658–665, May 1994.

[32] K. Rizk, J. Wagen, and F. Gardiol, "Two-dimensional ray-tracing modeling for propagation prediction in microcellular environments," *IEEE Trans. Veh. Technol.*, vol. 46, no. 2, pp. 508–518, May 1997.

[33] K. Rizk, J. Wagen, and F. Gardiol, "Influence of database accuracy on two-dimensional ray-tracing-based predictions in urban microcells," *IEEE Trans. Veh. Technol.*, vol. 49, no. 2, pp. 631–642, Jul. 2000.

[34] G. E. Athanasiadou and A. R. Nix, "Investigation into the sensitivity of the power predictions of a microcellular ray tracing propagation model," *IEEE Trans. Veh. Technol.*, vol. 49, no. 4, pp. 1140–1151, Jul. 2000.

[35] G. E. Athanasiadou, A. R. Nix, and J. P. McGeehan, "A microcellular ray-tracing propagation model and evaluation of its narrow-band and wide-band predictions," *IEEE J. Sel. Areas Commun.*, vol. 18, no. 3, pp. 322–335, Mar. 2000.

[36] J.-P. Rossi and Y. Gabillet, "A mixed ray launching/tracing method for full 3-D UHF propagation modeling and comparison with wide-band measurements," *IEEE Trans. Antennas Propag.*, vol. 50, no. 4, pp. 517–523, Apr. 2002.

[37] D. He, G. Liang, J. Portilla, and T. Riesgo, "A novel method for radio propagation simulation based on automatic 3D environment reconstruction," in *Proc. 6th Eur. Conf. Antennas Propag. (EUCAP)*, 2012, pp. 1445–1449.

[38] F. Lafarge, X. Descombes, J. Zerubia, and M. Pierrot-Deseilligny, "An automatic building reconstruction method: A structural approach using high resolution satellite images," in *Proc. Int. Conf. Image Process.*, 2006, pp. 1205–1208.

[39] Z. Yun, M. F. Iskander, S. Y. Lim, D. He, and R. Martinez, "Radio wave propagation prediction based on 3-D building structures extracted from 2-D images," *IEEE Antennas Wireless Propag. Lett.*, vol. 6, pp. 557–559, 2007.

[40] Z. Yun, M. F. Iskander, and S. Y. Lim, "The effect of 3D building reconstruction errors on propagation prediction using geospatial data in cyberspace," in *Proc. IEEE Antennas Propag. Soc. Int. Symp.*, 2009, pp. 1–4.

[41] Z. Yun, S. Y. Lim, and M. F. Iskander, "Use of geospatial resources for radio propagation prediction in urban areas," *IEEE Antennas Wireless Propag. Lett.*, vol. 8, pp. 587–591, 2009.

[42] Z. Yun, S. Y. Lim, and M. F. Iskander, "Modeling three-dimensional terrain in urban propagation environment using geospatial data in cyberspace," in *Proc. IEEE Antennas Propag. Soc. Int. Symp.*, 2010, pp. 1–4.

[43] A. Aschrafi, P. Wertz, M. Layh, F. M. Landstorfer, G. Wolfle, and R. Wahl, "Impact of building database accuracy on predictions with wave propagation models in urban scenarios," in *Proc. 63rd Veh. Technol. Conf.*, vol. 6, 2006, pp. 2681–2685.

[44] C. Zhongqiang, A. Delis, and H. L. Bertoni, "Building footprint simplification techniques and their effects on radio propagation predictions," *Comput. J.*, vol. 47, no. 1, pp. 103–133, 2004.

[45] T. Kurner and A. Meier, "Prediction of outdoor and outdoor-to-indoor coverage in urban areas at 1.8 GHz," *IEEE J. Sel. Areas Commun.*, vol. 20, no. 3, pp. 496–506, Apr. 2002.

[46] S. Popov, V. Glazunov, M. Chuvatov, and A. Purii, "Raster to vector map convertion by irregular grid of heights," in *Proc. 26th Conf. Open Innov. Assoc. (FRUCT)*, 2020, pp. 386–391.

[47] H. L. Bertoni, S. A. Torrico, and G. Liang, "Predicting the radio channel beyond second-generation wireless systems," *IEEE Antennas Propag. Mag.*, vol. 47, no. 4, pp. 28–40, Aug. 2005.

[48] P. Pongsilamanee and H. L. Bertoni, "Specular and nonspecular scattering from building facades," *IEEE Trans. Antennas Propag.*, vol. 52, no. 7, pp. 1879–1889, Jul. 2004.

[49] P. Kyösti, J. Lehtomäki, J. Medbo, and M. Latva-Aho, "Map-based channel model for evaluation of 5G wireless communication systems," *IEEE Trans. Antennas Propag.*, vol. 65, no. 12, pp. 6491–6504, Dec. 2017.

[50] N. C. Goncalves and L. M. Correia, "A propagation model for urban microcellular systems at the UHF band," *IEEE Trans. Veh. Technol.*, vol. 49, no. 4, pp. 1294–1302, Jul. 2000.

[51] E. M. Vitucci *et al.*, "Ray tracing RF field prediction: An unforgiving validation," *Int. J. Antennas Propag.*, vol. 2015, pp. 1–11, Aug. 2015.

[52] N. Z. Mohammed, A. Ghazi, and H. E. Mustafa, "Positional accuracy testing of Google earth," *Int. J. Multidiscip. Sci. Eng.*, vol. 4, no. 6, pp. 6–9, 2013.

[53] G. Pulighe, V. Baiocchi, and F. Lupia, "Horizontal accuracy assessment of very high resolution Google earth images in the city of Rome, Italy," *Int. J. Digit. Earth*, vol. 9, no. 4, pp. 342–362, 2016.

[54] M. A. Goudarzi and R. J. Landry, "Assessing horizontal positional accuracy of Google earth imagery in the City of Montreal, Canada," *Geodesy Cartography*, vol. 43, no. 2, pp. 56–65, 2017.

[55] C. U. Paredes-Hernández, W. E. Salinas-Castillo, F. Guevara-Cortina, and X. Martinez-Becerra, "Horizontal positional accuracy of Google earth's imagery over rural areas: A study case in Tamaulipas, Mexico," *Boletim de Ciências Geodésicas*, vol. 19, no. 4, pp. 588–601, 2013.

[56] M. A. El-Ashmawy, "Testing the positional accuracy of OpenStreetMap data for mapping applications," *Geodesy Cartography*, vol. 42, no. 1, pp. 25–30, 2015.

[57] H. Fan, A. Zipf, Q. Fu, and P. Neis, "Quality assessment for building footprints data on OpenStreetMap," *Int. J. Geograph. Inf. Sci.*, vol. 28, no. 4, pp. 700–719, 2014.

[58] H. T. Friis, "A note on a simple transmission formula," *Proc. IRE*, vol. 34, no. 5, pp. 254–256, 1946.

[59] V. Degli-Esposti, D. Guiducci, A. de'Marsi, P. Azzi, and F. Fuschini, "An advanced field prediction model including diffuse scattering," *IEEE Trans. Antennas Propag.*, vol. 52, no. 7, pp. 1717–1728, Jul. 2004.

[60] M. C. Lawton and J. P. McGeehan, "The application of a deterministic ray launching algorithm for the prediction of radio channel characteristics in small-cell environments," *IEEE Trans. Veh. Technol.*, vol. 43, no. 4, pp. 955–969, Nov. 1994.

[61] S. Y. Tan and H. S. Tan, "UTD propagation model in an urban street scene for microcellular communications," *IEEE Trans. Electromagn. Compat.*, vol. 35, no. 4, pp. 423–428, Nov. 1993.

[62] H. R. Anderson, "A ray-tracing propagation model for digital broadcast systems in urban areas," *IEEE Trans. Broadcast.*, vol. 39, no. 3, pp. 309–317, Sep. 1993.

[63] S. Kim *et al.*, "Radio propagation measurements and prediction using three-timensional ray tracing in urban environments at 908 MHz and 1.9 GHz," *IEEE Trans. Veh. Technol.*, vol. 48, no. 3, pp. 931–946, May 1999.

[64] O. Landron, M. J. Feuerstein, and T. S. Rappaport, "A comparison of theoretical and empirical reflection coefficients for typical exterior wall surfaces in a mobile radio environment," *IEEE Trans. Antennas Propag.*, vol. 44, no. 3, pp. 341–351, Mar. 1996.

[65] J. P. Berg, "A recursive method for street microcell path loss calculations," in *Proc. Int. Symp. Pers., Indoor Mobile Radio Commun.*, vol. 1, 1995, pp. 140–143.

[66] R. Luebbers, "Finite conductivity uniform GTD versus knife edge diffraction in prediction of propagation path loss," *IEEE Trans. Antennas Propag.*, vol. AP-32, no. 1, pp. 70–76, Jan. 1984.

[67] V. Erceg, S. J. Fortune, J. Ling, A. J. Rustako, and R. A. Valenzuela, "Comparisons of a computer-based propagation prediction tool with experimental data collected in urban microcellular environments," *IEEE J. Sel. Areas Commun.*, vol. 15, no. 4, pp. 677–684, May 1997.

[68] G. Liang and H. L. Bertoni, "A New Approach to 3-D Ray Tracing for Propagation Prediction in Cities," *IEEE Trans. Antennas Propag.*, vol. 46, no. 6, pp. 853–863, Jun. 1998.

[69] C.-H. Teh, B.-K. Chung, and E.-H. Lim, "An accurate and efficient 3-D shooting-and-bouncing-polygon ray tracer for radio propagation modeling," *IEEE Trans. Antennas Propag.*, vol. 66, no. 12, pp. 7244–7254, Dec. 2018.

[70] B. E. Gschwendtner and F. M. Landstorfer, "3-D propagation modelling in microcells including terrain effects," in *Proc. 6th Int. Symp. Pers. Indoor Mobile Radio Commun.*, vol. 2, 1995, pp. 532–536.

[71] S. Y. Tan and H. S. Tan, "Propagation model for microcellular communications applied to path loss measurements in Ottawa City Streets," *IEEE Trans. Veh. Technol.*, vol. 44, no. 2, pp. 313–317, Jul. 1995.

[72] S. Y. Tan and H. S. Tan, "A microcellular communications propagation model based on the uniform theory of diffraction and multiple image theory," *IEEE Trans. Antennas Propag.*, vol. 44, no. 10, pp. 1317–1326, Oct. 1996.

[73] H. R. Anderson, "Building corner diffraction measurements and predictions using UTD," *IEEE Trans. Antennas Propag.*, vol. 46, no. 2, pp. 292–293, Feb. 1998.

[74] C. Oestges, B. Clerckx, L. Raynaud, and D. Vanhoenacker-Janvier, "Deterministic channel modeling and performance simulation of microcellular wide-band communication systems," *IEEE Trans. Veh. Technol.*, vol. 51, no. 6, pp. 1422–1430, Nov. 2002.

[75] F. Mani and C. Oestges, "Ray-tracing evaluation of diffuse scattering in an outdoor scenario," in *Proc. 5th Eur. Conf. Antennas Propag. (EUCAP)*, 2011, pp. 3439–3443.

[76] "Effects of building materials and structures on radiowave propagation above about 100 MHz," Int. Telecommun. Union, Geneva, Switzerland, ITU Recommandation P.2040-1, 2015.

[77] S. S. Zhekov, O. Franek, and G. F. Pedersen, "Dielectric properties of common building materials for ultrawideband propagation studies [measurements corner]," *IEEE Antennas Propag. Mag.*, vol. 62, no. 1, pp. 72–81, Feb. 2020.

[78] S. Stavrou and S. R. Saunders, "Review of constitutive parameters of building materials," in *Proc. 12th Int. Conf. Antennas Propag.*, vol. 1, 2003, pp. 211–215.

[79] D. Ferreira, I. Cuiñas, R. F. S. Caldeirinha, and T. R. Fernandes, "A review on the electromagnetic characterisation of building materials at micro- and millimetre wave frequencies," in *Proc. 8th Eur. Conf. Antennas Propag. (EuCAP)*, 2014, pp. 145–149.

[80] D. Ferreira, R. F. S. Caldeirinha, T. R. Fernandes, and I. Cuiñas, "Hollow clay brick wall propagation analysis and modified brick design for enhanced Wi-Fi coverage," *IEEE Trans. Antennas Propag.*, vol. 66, no. 1, pp. 331–339, Jan. 2018.

[81] D. Katz, N. Blaunstein, M. Hayakawa, and Y. Sanoh Kishiki, "The design of radio maps in Tokyo City based on stochastic multi-parametric and deterministic ray-tracing approaches [wireless corner]," *IEEE Antennas Propag. Mag.*, vol. 51, no. 5, pp. 200–208, Oct. 2009.

[82] S. Y. Seidel and T. S. Rappaport, "Site-specific propagation prediction for wireless in-building personal communication system design," *IEEE Trans. Veh. Technol.*, vol. 43, no. 4, pp. 879–891, Nov. 1994.

[83] J. Jemai, P. C. F. Eggers, G. F. Pedersen, and T. Kurner, "Calibration of a UWB sub-band channel model using simulated annealing," *IEEE Trans. Antennas Propag.*, vol. 57, no. 10, pp. 3439–3443, Oct. 2009.

[84] R. G. Kouyoumjian, "Asymptotic high-frequency methods," *Proc. IEEE*, vol. 53, no. 8, pp. 864–876, Aug. 1965.

[85] O. Franek, S. Zhang, K. Olesen, P. C. F. Eggers, C. Byskov, and G. F. Pedersen, "Numerical modeling of ultrawideband propagation along a wind turbine blade," *IEEE Trans. Antennas Propag.*, vol. 66, no. 12, pp. 6570–6579, Dec. 2018.

[86] M. S. L. Mocker *et al.*, "Combination of a full-wave method and ray tracing for radiation pattern simulations of antennas on vehicle roofs," in *Proc. 9th Eur. Conf. Antennas Propag. (EuCAP)*, 2015, pp. 1–5.

[87] F. Ikegami, T. Takeuchi, and S. Yoshida, "Theoretical prediction of mean field strength for urban mobile radio," *IEEE Trans. Antennas Propag.*, vol. 39, no. 3, pp. 299–302, Mar. 1991.

[88] V. Erceg, A. J. Rustako, and R. S. Roman, "Diffraction around corners and its effects on the microcell coverage area in urban and suburban environments at 900 MHz, 2 GHz, and 6 GHz," *IEEE Trans. Veh. Technol.*, vol. 43, no. 3, pp. 762–766, Aug. 1994.

[89] J. Nuckelt, T. Abbas, F. Tufvesson, C. Mecklenbrauker, L. Bernado, and T. Kurner, "Comparison of ray tracing and channel-sounder measurements for vehicular communications," in *Proc. IEEE 77th Veh. Technol. Conf.*, 2013, pp. 1–5.

[90] V. Degli-Esposti *et al.*, "A semi-deterministic model for outdoor-to-indoor prediction in urban areas," *IEEE Antennas Wireless Propag. Lett.*, vol. 16, pp. 2412–2415, 2017.

[91] T. A. Russell, T. S. Rappaport, and C. W. Bostian, "Use of a building database in prediction of three-dimensional diffraction," in *Proc. 42nd Veh. Technol. Conf.*, vol. 2, 1992, pp. 943–946.

[92] D. Didascalou, M. Dottling, N. Geng, and W. Wiesbeck, "An approach to include stochastic rough surface scattering into deterministic ray-optical wave propagation modeling," *IEEE Trans. Antennas Propag.*, vol. 51, no. 7, pp. 1508–1515, Jul. 2003.

[93] J. Thrane, D. Zibar, and H. L. Christiansen, "Comparison of empirical and ray-tracing models for mobile communication systems at 2.6 GHz," in *Proc. IEEE 90th Veh. Technol. Conf.*, 2019, pp. 1–5.

[94] Z. Yun, Z. Zhang, and M. F. Iskander, "A ray-tracing method based on the triangular grid approach and application to propagation prediction in urban environments," *IEEE Trans. Antennas Propag.*, vol. 50, no. 5, pp. 750–758, May 2002.

[95] J. Maurer, T. Fugen, T. Schafer, and W. Wiesbeck, "A new inter-vehicle communications (IVC) channel model," in *Proc. IEEE 60th Veh. Technol. Conf.*, vol. 1, 2004, pp. 9–13.

[96] T. Jämsä, P. Kyösti, and K. Kusume, "Initial channel models based on measurements," Mobile and Wireless Communications Enablers for the Twenty-Twenty Information Society (METIS 2020 Project), Rep. ICT-317669-METIS/D1.2, 2014. [Online]. Available: https://metis2020.com/wp-content/uploads/deliverables/METIS_D1.2_v1.pdf

[97] C. Bergljung and L. G. Olsson, "Rigorous diffraction theory applied to street microcell propagation," in *Proc. IEEE Global Telecommun. Conf.*, vol. 2, 1991, pp. 1292–1296.

[98] C. Bergljung and L. G. Olsson, "A comparison of solutions to the problem of diffraction of a plane wave by a dielectric wedge," in *Proc. IEEE Antennas Propag. Soc. Int. Symp.*, vol. 4, 1992, pp. 1861–1864.

[99] P. D. Holm, "A new heuristic UTD diffraction coefficient for nonperfectly conducting wedges," *IEEE Trans. Antennas Propag.*, vol. 48, no. 8, pp. 1211–1219, Aug. 2000.

[100] D. Bilibashi, E. M. Vitucci, and V. Degli-Esposti, "Dynamic ray tracing: Introduction and concept," in *Proc. 14th Eur. Conf. Antennas Propag. (EuCAP)*, 2020, pp. 1–5.

[101] A. Karstensen, W. Fan, F. Zhang, J. Ø. Nielsen, and G. F. Pedersen, "Analysis of simulated and measured indoor channels for mm-Wave beamforming applications," *Int. J. Antennas Propag.*, vol. 2018, pp. 1–17, Jan. 2018.

ALLAN WAINAINA MBUGUA received the B.Sc. degree in telecommunication and information engineering from the Jomo Kenyatta University of Agriculture and Technology, Juja, Kenya, in 2014, and the M.Sc. degree in telecommunications engineering from the University of Cassino and Southern Lazio, Cassino, Italy, in 2018. He is currently pursuing the Ph.D. degree with Huawei Techonologies Duesseldorf GmbH, Munich Research Center, Munich, Germany, and the Antennas, Propagation and Millimetre-Wave Systems (APMS) Section, Aalborg University, Aalborg, Denmark, with a focus on millimeter-wave radio channel measurements and channel characterization.

YUN CHEN received the B.Sc., M.Sc., and Ph.D. degrees from the University of Duisburg-Essen, Germany, in 2006, 2008, and 2012, respectively. He was with Rohde and Schwarz and Fraunhofer Research Society, Munich, Germany. He is currently working as a Project Manager with Huawei Technologies Duesseldorf GmbH, Munich, Germany, with a focus on site-specific channel modeling and technologies research on 5G system testing.

LESZEK RASCHKOWSKI received the Dipl.-Ing. (M.S.) degree in electrical engineering from Technische Universität Berlin, Germany, in 2012. He is currently employed as a Research Associate and a Project Manager with Fraunhofer Heinrich Hertz Institute, Berlin, Germany. He is working on several research projects in the field of wireless communications. In addition, he is actively contributing to 3GPP standardization work related to the radio access network as a regular delegate since 2013. At the moment, he works on the integration of non-terrestrial networks (satellite constellations) into the 5G ecosystem. His research interests include measuring, modeling and simulating radio propagation channels, as well as performance analysis of wireless communication systems. This encompasses 3D MIMO, deployments in industrial factory halls, aerial vehicles (drones) and satellites.

LARS THIELE received the Dipl.-Ing. (M.S.) degree in electrical engineering from the Technische Universität Berlin, Berlin, Germany, in 2005, and the Dr.-Ing. (Ph.D.) degree from the Technical University of Munich (TUM) in 2013. He joined the Fraunhofer Heinrich Hertz Institute (HHI) in September 2005. He contributed to receiver and transmitter optimization under limited feedback, performance analysis for MIMO and massive-MIMO transmission in cellular ODFM systems, fair-resource allocation and CoMP transmission under constrained CSIT. He has authored and coauthored more than 50 conference and journal papers as well as a couple of book chapters in the area of mobile communications. Since 2015, he has been actively participating in 3GPP RAN1. He leads the System Level Innovation Research Group, Fraunhofer HHI. The main focus of the group lies in the field of 5G channel modeling, signal processing on PHY and MAC-layer as well as bit-level and system-level simulation for 5G and beyond. A list of publications can be found at https://scholar.google.de/citations?user=cGgvIqUAAAAJ&hl=de

STEPHAN JAECKEL (Member, IEEE) was born in Freiberg, Germany, in 1982. He received the M.Eng. degree in information and communications technology from Hochschule für Telekommunikation, Leipzig, Germany, in 2007, and the Dr.-Ing. (Ph.D.) degree in electrical, electronics and communications engineering from the Technische Universität Ilmenau, Ilmenau, Germany, in 2017. In 2007, he joined the Fraunhofer Heinrich Hertz Institute, Berlin, Germany, where he worked on the measurement-based performance analysis of cooperative mobile communication systems. In 2010, he created the QuaDRiGa radio propagation model which also became the topic of his dissertation. In 2020, he launched his own business to develop strategies for integrating emerging technology trends such as machine learning, edge computing or IoT with the 5G physical layer. His research interests included measurements and data analysis in heterogeneous multicell networks, including relays as well as channel modeling for terrestrial and satellite systems.

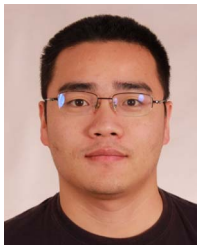

WEI FAN (Senior Member, IEEE) received the B.E. degree from the Harbin Institute of Technology, Harbin, China, in 2009, the dual master's degrees (Hons.) from the Politecnico di Torino, Turin, Italy, and the Grenoble Institute of Technology, Grenoble, France, in 2011, and the Ph.D. degree from Aalborg University, Aalborg, Denmark, in 2014. In 2011, he joined Intel Mobile Communications, Aalborg, as a Research Intern. He conducted a three-month internship with Keysight Technologies, Oulu, in 2014. He is currently an Associate Professor with the Antennas, Propagation and Millimetre-Wave Systems (APMS) Section, Aalborg University. His current research interests include over-the-air testing of multiple antenna systems and radio channel sounding, parameter estimation, modeling, and emulation.